




Article

A Novel Localization in Human Large Extracellular Vesicles for the EGF-CFC Founder Member CRIPTO and Its Biological and Therapeutic Implications

Francesca Mantile ¹, Matic Kisovec ², Giorgia Adamo ³, Daniele P. Romancino ³, Matej Hočevár ⁴, Darja Božič ^{5,6}, Apolonija Bedina Zavec ², Marjetka Podobnik ², Maria Patrizia Stoppelli ¹, Annamaria Kisslinger ⁷, Antonella Bongiovanni ³, Veronika Kralj-Iglič ^{5,6} and Giovanna L. Liguori ^{1,*}

¹ Institute of Genetics and Biophysics (IGB) “Adriano Buzzati Traverso”, National Research Council (CNR) of Italy, 80131 Naples, Italy; fmantile185@gmail.com (F.M.); mpatrizia.stoppelli@igb.cnr.it (M.P.S.)

² Department of Molecular Biology and Nanobiotechnology, National Institute of Chemistry, SI-1000 Ljubljana, Slovenia; matic.kisovec@ki.si (M.K.); polona.bedina@ki.si (A.B.Z.); marjetka.podobnik@ki.si (M.P.)

³ Institute for Research and Biomedical Innovation (IRIB), CNR, 90146 Palermo, Italy; giorgia.adamo@irib.cnr.it (G.A.); daniele.romancino@irib.cnr.it (D.P.R.); antonella.bongiovanni@irib.cnr.it (A.B.)

⁴ Department of Physics and Chemistry of Materials, Institute of Metals and Technology, SI-1000 Ljubljana, Slovenia; matej.hocevar@imt.si

⁵ Faculty of Health Sciences, University of Ljubljana, SI-1000 Ljubljana, Slovenia; darja.bozic@biaseparations.com (D.B.); veronika.iglic@fe.uni-lj.si (V.K.-I.)

⁶ Faculty of Electrical Engineering, University of Ljubljana, SI-1000 Ljubljana, Slovenia

⁷ Institute of Experimental Endocrinology and Oncology (IEOS), National Research Council (CNR) of Italy, 80131 Naples, Italy; a.kisslinger@ieos.cnr.it

* Correspondence: giovanna.liguori@igb.cnr.it



Citation: Mantile, F.; Kisovec, M.; Adamo, G.; Romancino, D.P.; Hočevár, M.; Božič, D.; Bedina Zavec, A.; Podobnik, M.; Stoppelli, M.P.; Kisslinger, A.; et al. A Novel Localization in Human Large Extracellular Vesicles for the EGF-CFC Founder Member CRIPTO and Its Biological and Therapeutic Implications. *Cancers* **2022**, *14*, 3700. <https://doi.org/10.3390/cancers14153700>

Academic Editors: Kebin Hu, Yandong Zhou and Ling Lin

Received: 13 June 2022

Accepted: 21 July 2022

Published: 29 July 2022

Publisher's Note: MDPI stays neutral with regard to jurisdictional claims in published maps and institutional affiliations.



Copyright: © 2022 by the authors. Licensee MDPI, Basel, Switzerland. This article is an open access article distributed under the terms and conditions of the Creative Commons Attribution (CC BY) license (<https://creativecommons.org/licenses/by/4.0/>).

Simple Summary: During tumorigenesis, communication among cells is fundamental. Tumor cells can communicate through the release of extracellular vesicles (EVs), carrying active mediators, that are able to move in the extracellular space and in the body fluids, thereby reaching cells different from the ones of origin. Tumor-derived EVs, upon interaction with tumor target cells, can profoundly change cell characteristics and behavior. Here, we isolated EVs released from human teratocarcinoma cells and we uncovered their ability to inhibit the cell migration of glioblastoma (GBM) cells. Teratocarcinoma EVs contain the oncofetal protein CRIPTO, that is involved in the observed reduction of GBM cell migration. Our results suggest a novel localization and function for CRIPTO in large EVs, and give precious hints for the development of novel therapeutic approaches, based on the control of tumor cell migration, to ultimately improve prognosis and quality of life of GBM patients.

Abstract: Tumor growth and metastasis strongly rely on cell–cell communication. One of the mechanisms by which tumor cells communicate involves the release and uptake of lipid membrane encapsulated particles full of bioactive molecules, called extracellular vesicles (EVs). EV exchange between cancer cells may induce phenotype changes in the recipient cells. Our work investigated the effect of EVs released by teratocarcinoma cells on glioblastoma (GBM) cells. EVs were isolated by differential centrifugation and analyzed through Western blot, nanoparticle tracking analysis, and electron microscopy. The effect of large EVs on GBM cells was tested through cell migration, proliferation, and drug-sensitivity assays, and resulted in a specific impairment in cell migration with no effects on proliferation and drug-sensitivity. Noticeably, we found the presence of the EGF-CFC founder member CRIPTO on both small and large EVs, in the latter case implicated in the EV-mediated negative regulation of GBM cell migration. Our data let us propose a novel route and function for CRIPTO during tumorigenesis, highlighting a complex scenario regulating its effect, and paving the way to novel strategies to control cell migration, to ultimately improve the prognosis and quality of life of GBM patients.

Keywords: extracellular vesicles; microvesicles; CRIPTO; teratocarcinoma; glioblastoma; inhibition of cell migration; cancer therapy

1. Introduction

Cancer cell–cell communication is crucial for tumor growth and metastasis. Tumors are very far from being isolated entities, but rather strongly rely on communication between tumoral cells with each other as well as with different types of non-transformed cells which compose the tumor microenvironment. Over the past 10 years, a new paradigm has emerged involving extracellular vesicles (EVs) as key factors for cell communication. EVs are lipid membrane encapsulated structures full of bioactive components released by cells by either blebbing of the cell membrane or by the endocytic pathway. EVs are able to be transported by body fluids and deliver molecules very far from the cell of origin, into target cells in which EVs can induce specific responses [1,2]. Different operational terms are used to distinguish the various subtypes of EVs with respect to physical characteristics (size, density), biochemical composition, or cell of origin. Among the most used terms, there are small EVs (sEVs) and medium/large EVs, m/IEVs, or simply large EVs (lEVs), which indicate vesicles with a size approximately smaller (sEVs) and larger (lEVs) of 200–250 nm (depending also on the type of analysis). lEVs can also reach 1–2 micron in size [2,3]. Due to their intriguing features, EVs emerged as a novel liquid biopsy resource of new biomarkers to be used in cancer diagnosis, prognosis, and treatment as well as promising carriers for the delivery of new therapeutic molecules against cancer.

CRIPTO is the founder member of the vertebrate Epidermal Growth Factor-Cripto/FRL-1/Cryptic (EGF-CFC) gene family involved in embryonic and post-natal development [4,5]. In vivo mouse *Cripto* gene targeting revealed a key role of this gene during embryogenesis in A/P polarity definition, mesoderm formation including the mouse primary organizer, early anterior neural patterning, and secondary organizer development [6–9]. Moreover, the homologous recombination in embryonic stem (ES) cells demonstrated a specific role of *Cripto* in cardiomyocytes differentiation [10,11]. *Cripto* is also required in extraembryonic tissues for embryo implantation, as demonstrated by the in utero transplantation of embryos with *Cripto*-depleted trophoblast cells [12]. In the adult, *Cripto* expression levels are largely negligible at the tissue level. The apparent loss of *Cripto* gene expression in adult tissues might reflect the rarity of the cells expressing it, rather than its absence per se [13]. In humans, CRIPTO distribution appears restricted to stem cell niches and the small subpopulation of adult somatic cells, being implicated in stem cell compartment of hierarchically organized tissues (i.e., hematopoietic system, gastrointestinal epithelium), in normal cyclic regenerative processes as well as in injury/regeneration settings [13]. CRIPTO protein is also detectable in the serum of the majority of individuals in a population-based sample [14]. High CRIPTO expression levels, instead, have been related to tumorigenesis and poor prognosis in an increasing number of cancers, as for example, melanoma, breast, lung, esophageal, gastric, colon, hepatocellular, pancreatic, renal, prostate, and bladder carcinomas [13,15,16]. In many of these, CRIPTO expression has been mainly detected in cancer stem cells (CSCs), suggesting its role in CSC compartment regulation [13]. On the other side, CRIPTO is also able to induce many tumorigenic features, such as Epithelial-Mesenchymal transition (EMT), tumor cell proliferation, migration, and tumor neovascularization [15,17].

Cripto, as with all the EGF-CFC factors, is an extracellular protein characterized by two six-cysteine motifs. The first one is a pseudo EGF-like motif, which differs from the canonical one because of the first two adjacent cysteines and the inability to interact with the EGF receptors; and the second one is a CFC motif, which is unique to this protein family [4,5]. Moreover, *Cripto* contains at the C-terminus a hydrophobic domain bearing a consensus sequence for a glycosylphosphatidylinositol (GPI) anchor attachment. GPI anchorage ensures linking to the outer layer of the plasma membrane, and can be also cleaved, releasing extracellularly an active *Cripto* protein [18,19]. Therefore, *Cripto* can

act both *in cis* as a membrane bound protein as well as *in trans* as a soluble factor. Very recently, Hu and coauthors reported also the presence of CRIPTO on the membrane of the sEVs released by perihilar cholangiocarcinoma (PHCCA) cells [20].

CRIPTO was isolated in human teratocarcinoma NTERA2 cells, and, for this reason, it is also named *TERATOCARCINOMA DERIVED GROWTH FACTOR 1* or *TDGF1* [21,22]. Teratocarcinomas are one of the most common types of testicular germ cell tumors in young men, and are composed of embryonal carcinoma stem cells and various layers of differentiated cells [23]. The NTERA2 teratocarcinoma cell line was established from a nude mouse xenograft of the TERA2 cell line, derived from a lung metastasis of a testicular teratocarcinoma. In the presence of retinoic acid (RA), NTERA2 cells differentiate into neuronal postmitotic cells, resembling neural stem/progenitor cell behavior [23]. Therefore, NTERA2 cells have been extensively used as the model system to mimic neural stem/progenitor cells.

GBM is the most common and aggressive primary brain tumor in adults, with a prognosis of 12–15 months and just 3–5% of survival over 5 years [24]. This is mainly because most patients suffer recurrence after treatment that mainly consists of maximal resection followed by radio- and chemotherapy with TMZ [24,25]. Various studies suggested that neural stem cells (NSCs) might be the cells of origin of GBM, which arises from the migration of mutated astrocyte-like NSCs [26–29]. Previous reports indicated that NSCs target intracranial glioma and could serve as a delivery vector to the anti-glioma therapy [30]. Moreover, a conditioned medium isolated from NSCs, is able to affect GBM cell behavior, by inhibiting glioma cell growth, invasion, and migration *in vitro* and attenuate the tumor growth *in vivo* [31]. Interestingly, NTERA2 cells also show a glioma tropism in animal models and were proposed as a cell-based gene delivery, definitely more suitable than NSCs, to inhibit the proliferation and migration of gliomas [32,33]. Moreover, also, a conditioned medium from pristine NTERA2 cells is able to affect GBM development [32].

In the present study, we aimed to investigate the presence of CRIPTO in teratocarcinoma EVs as well as its functional significance. We chose as a model system the NTERA2 teratocarcinoma cell line, as vesicle producing cells, in which CRIPTO was originally identified and is strongly expressed, and the U87 GBM cells as target cells to use in functional assays. To our best knowledge, this is the first report on EVs isolated from the NTERA2 teratocarcinoma cells. Functional characterization of the NTERA2 IEVs unraveled a specific role in inhibiting the migration of U87 GBM cells, without affecting cell proliferation or inducing chemoresistance. Our analysis demonstrated the presence of CRIPTO in both NTERA2 sEVs and IEVs, with a strong enrichment in IEVs with respect to the small ones. Finally, our data suggest the involvement of the EV-associated CRIPTO protein in the reduction of U87 GBM cell migration induced by NTERA2 IEVs, paving the way to the possible use of EV-associated CRIPTO as a key player in GBM therapy.

2. Materials and Methods

2.1. Cell Culture

The teratocarcinoma cell line NTERA2 was purchased from ATCC (ATCC-CRL-1973), whereas the glioblastoma cell line U87 was purchased from Merck (89081402, Kenilworth, NJ, USA). Cells were cultured in Dulbecco's Modified Eagle's Medium (DMEM) supplemented with 10% (V/V) fetal bovine serum (FBS), penicillin (100 U/mL), and streptomycin (100 mg/mL) at 37 °C in a humidified atmosphere (5% CO₂). All cell culture media and reagents were provided by Gibco (Invitrogen, Carlsbad, CA, USA). For EV isolation, cells were seeded in 150 mm culture plates (Corning, 430599, New York, NY, USA) at a cell density of approximately 1×10^4 cells/cm² (U87) or 2.5×10^4 cells/cm² (NTERA2) and cultured for 24 h as described above. After that, cells were washed twice with phosphate-buffered saline (PBS) and cultured in DMEM supplemented with 10% EV-depleted FBS for 48 h. The EV-depleted FBS was prepared starting from 60% FBS diluted in DMEM by ultracentrifugation at $118,000 \times g$ for 16 h at 4 °C to remove the EVs present in the serum. After 48 h, cell culture was collected. For each EV preparation, culture medium was

collected from about 1.7×10^8 NTERA2 cells or from 7×10^7 U87 cells (used as control for EV isolation). Cell viability at the time of collection ranged from 95% to 100%, estimated by direct cell counting after trypan blue staining.

2.2. Extracellular Vesicle Isolation

EVs were isolated by differential centrifugation [34]. In brief, the conditioned medium was collected in Falcon tubes (Corning Falcon, 352070, New York, NY, USA), and centrifuged twice at $300 \times g$, 4°C for 10 min. Supernatant fractions were further centrifuged twice at $2000 \times g$, 4°C for 10 min to eliminate cell debris. Large extracellular vesicles (IEVs) were pelleted by centrifugation at $10,000 \times g$ at 4°C for 30 min in 14 mL polypropylen tubes (Falcon, 352059) in J20 XP Beckman centrifuge, using a J25.50 rotor, followed by washing with PBS. Small extracellular vesicles (sEVs) were pelleted from supernatant by ultracentrifugation at $118,000 \times g$, 4°C for 70 min, in 38.5 mL polypropylen tubes (Beckmann coulter, 326823, Brea, CA, USA) in Optima XE, Beckman ultracentrifuge using SW28 rotor, followed by washing with PBS. IEVs and sEVs were resuspended in 50 μL PBS for further analysis. The protein content of EV samples was measured using the BCA Protein Assay Kit (Thermo Fisher Scientific, Waltham, MA, USA).

2.3. Cell Lysate Preparation

Cells were lysed with a Radioimmunoprecipitation Assay (RIPA) buffer (50 mM Tris-HCl at pH 8, 150 mM NaCl, 1 mM EDTA pH 8, 1% Triton X-100) supplemented with Complete Protease Inhibitor Mixture tablets (Roche Diagnostics S-4693159001, Basilea, Switzerland). The protein concentration of cell lysates was measured using the Bradford Protein Assay (Biorad, Segrate, Italy).

2.4. Western Blot

Samples in reducing the Laemmli buffer were boiled at $95\text{--}100^\circ\text{C}$ for 5 min and separated by sodium dodecyl-sulfate polyacrylamide gel electrophoresis (SDS-PAGE) (12%). Then, proteins were transferred to polivinilidenfluoro (PVDF) membranes, and the membranes were blocked with 5% milk in TBS-T (50 mM Tris HCl pH 8.0, 150 mM NaCl with 0.05% Tween 20) for 1 h at room temperature, followed by incubation overnight at 4°C with the following primary antibodies: anti-CRIPTO rabbit monoclonal (1:500 dilution, Abcam, 133236, Cambridge, UK); anti-HSP70 mouse monoclonal (1:500 dilution, Santa Cruz Biotechnology, clone W27, Dallas, TX, USA); anti- β Actin rabbit polyclonal (1:1000 dilution, SIGMA, A2066, Saint Louis, MO, USA); Calnexin rabbit polyclonal antibody (1:500 dilution, NovusBio NB100-1965); CD63 rabbit polyclonal antibody (1:500 dilution, Invitrogen, #PA5-92370, Waltham, MA, USA) in 5% milk in TBS-T. After washing in the TBS-T buffer, the membranes were incubated for 1 h at room temperature with a 1:10,000 dilution of goat anti-rabbit secondary antibody (SIGMA, 12-348) or anti-mouse secondary antibody in 5% milk in TBS-T. Membranes were then washed three times in the TBS-T buffer and chemiluminescence detection was performed using an enhanced Chemiluminescence Kit according to the manufacturer's protocol (Clarity Western ECL substrate, Biorad, 1705060, Segrate, Italy).

2.5. Scanning Electron Microscopy

Isolates were fixed overnight at 4°C in Karnovsky's fixative with modification composed of 2.5% glutaraldehyde, 0.4% formaldehyde, and phosphate buffer saline (PBS) at pH 7.4 (137 mM NaCl, 2.68 mM KCl, 10.14 mM Na_2HPO_4 , and 1.84 mM KH_2PO_4), and post-fixed the following day with OsO_4 , according to the protocol adopted from Lešer et al. 2007 [35]. Fixatives were removed in three rinsing steps using PBS (10 min incubation in each step). Then, samples were incubated in 2% OsO_4 for one hour, rinsed three times with distilled water (10 min incubation time in each step), and with saturated water solution of thiocarbohydrazide (15 min incubation time), rinsed three times with distilled water (10 min incubation time in each step), incubated again in 2% OsO_4 for 1 h, washed three

times with distilled water (10 min incubation time in each step), and dehydrated in graded series of ethanol (30–100%, 10 min in each solution). Absolute ethanol was replaced three times, treated by the graded series of hexamethyldisilazane (mixed 30% and 50% with absolute ethanol and pure, 10 min incubation time in each step), and finally air dried overnight. Fixed and dehydrated samples were Au/Pd coated by Precision Etching and Coating System or PECS (Gatan Inc 682, Pleasanton, CA, USA), and examined using a JSM-6500F Field Emission Scanning Electron Microscope (JEOL Ltd., Tokyo, Japan).

2.6. Nanoparticle Tracking Analysis

Nanoparticle size distribution and concentration were measured using a NanoSight NS300 (Malvern Panalytical, Malvern, UK). The instrument was equipped with a 488 nm laser, a high-sensitivity sCMOS camera, and a syringe pump. The IEVs and sEVs were diluted to generate a dilution in which 20–120 particles per frame were tracked to obtain a concentration within the recommended measurement range ($1\text{--}10 \times 10^8$ particles/mL). The results were based on five and two independent samples for NTERA2 and U87, respectively. For each sample, 5 experiment videos of 60 s duration were analyzed using a nanoparticle tracking analysis NTA 3.4 Build 3.4.003 (camera level 15–16) with syringe pump speed 60. A total of 1500 frames were examined per sample, which were captured and analyzed by applying instrument-optimized settings using a suitable detection threshold so that the observed particles were marked with a red cross and that no more than five blue crosses were seen. Further settings such as blur size and Max Jump Distance were set to “automatic” and viscosity was set to water (0.841–0.844 cP).

2.7. Cryogenic Transmission Electron Microscopy

Quantifoil® R 2/2 (or 1.2/1.3), 200 (Quantifoil Micro Tools GmbH, Großlobichau, Germany) EM grids were glow discharged for 60 s at 20 mA and positive polarity in air atmosphere (GloQube® Plus, Quorum, Laughton, UK). Vitrobot conditions were set to 4 °C, 95% relative humidity, blot time: 5 s, and blot force: 4. An amount of 2 µL of the sample suspension was applied to the grid, blotted, and plunge-frozen in liquid ethane with Vitrobot Mark IV (Thermo Fisher Scientific, Waltham, MA, USA). Samples were visualized under cryo conditions with a Falcon 3EC detector on a 200 kV microscope Glacios (Thermo Fisher Scientific, Waltham, MA, USA).

2.8. Flow Cytometry

NTERA2 cells were detached using 0.5% trypsin, counted, and resuspended in 5% FBS in PBS (1×10^6 cells were resuspended in a volume of 100 µl) and incubated with the primary anti-CRIPTO rabbit polyclonal antibody (Abcam, 19917) for 1 h in ice at dark. After washing twice with PBS, cells were incubated with the secondary antibody Alexa Fluor 594 donkey anti-rabbit (Invitrogen A21207) for 1 h in ice at dark. After washing twice with PBS, cells were resuspended in 5% FBS in PBS, filtered, and analyzed with the BD FACS ARIAM flow cytometer. Data were collected using BD FACSDiva software (v8.0.1 Becton Dickinson, Franklin Lakes, NJ, USA). For each sample, the data of 20,000 cells were collected.

2.9. Wound Healing Assay

U87 cells were seeded into Ibidi inserts (Ibidi, GmbH, Martinsried, Germany, 81176), and placed in 24-well plates (13,000 cell/well) in the complete medium (10% FBS; 100 U/mL penicillin and 100 mg/mL streptomycin in DMEM). After 24 h, the Ibidi inserts were removed, the cells were washed with PBS, and the complete medium was replaced with DMEM 2% EV-depleted FBS, penicillin (100 U/mL), and streptomycin (100 mg/mL). The following treatments were added to cells: 10 µg/mL of NTERA2-IEVs; 10 µg/mL of NTERA2-IEVs previously incubated 1 h at 4 °C with 1:100 anti-CRIPTO antibody (Abcam, ab 19917) (IEVs- α -CRIPTO); 10 µg/mL of NTERA2-IEVs previously incubated 1 h at 4 °C with 1:100 anti-rabbit IgG antibody (SIGMA, 12-348) (IEVs- α -IgG). As the control, non-treated cells were used. The closing of the wound was observed after 6 and

20 h. All treatments were performed in the presence of 2 $\mu\text{g}/\text{mL}$ mitomycin C to inhibit cell proliferation. ImageJ software (v1.51, Wayne Rasband, National Institutes of Health, USA, open source) was used to analyze the results. The relative wound healing area was calculated as (initial area—final area)/initial area. Three independent experiments were performed, each one in duplicate. Data are shown as means \pm standard error of the mean (s.e.m).

2.10. Cell Proliferation and Drug Sensitivity Assay

U87 cells were seeded in a volume of 100 μL at 5×10^2 cells/well in 96-well plates. After 24 h, the culture medium was replaced with DMEM 2% EV-depleted FBS, penicillin (100 U/mL), and streptomycin (100 mg/mL), and the following treatments were added to cells: 10 $\mu\text{g}/\text{mL}$ of NTERA2-IEVs; 10 $\mu\text{g}/\text{mL}$ of NTERA2-IEVs previously incubated 1 h at 4 °C with 1:100 anti-CRIPTO antibody (Abcam, 19997) (IEVs- α -CRIPTO); 10 $\mu\text{g}/\text{mL}$ of NTERA2-IEVs previously incubated 1 h at 4 °C with 1:100 anti-rabbit IgG antibody (SIGMA, 12-348) (IEVs- α -IgG). After incubation at 37 °C for 48 and 72 h, 20 μL of CellTiter 96[®] AQueous One Solution Reagent (Promega) was added, and the plates were incubated at 37 °C for 2 h. The reaction was stopped by the addition of 25 μL 10% SDS and the absorbance (A) at 490 nm was measured using a microtiter plate spectrophotometer. Values were expressed as means \pm s.e.m. of two independent experiments, each one performed in duplicate.

In drug sensitivity experiments, freshly prepared 100 μM of Temozolomide (TMZ; Sigma) was added to cells, in combination or not with NTERA2-IEVs. After incubation at 37 °C for 72 h, 20 μL of CellTiter 96[®] AQueous One Solution Reagent (Promega) was added, and the plates were incubated at 37 °C for 2 h. The number of viable cells in each sample was calculated as the percentage of viable cells after the treatment, with respect to the one found in the control with no TMZ.

2.11. Quality Management

The study has been performed in compliance with the VES4US Quality Management System [36] and following minimal instruction for studying the EVs (MISEV2018) [3]. Cell culture experiments have been conducted in accordance with the quality-based research guidelines previously identified [37,38].

2.12. Statistical Analysis

Student's *t*-test was used to determine the statistical significance of the quantitative results. Statistical significance was indicated by * = $p < 0.05$; ** = $p < 0.01$; *** = $p < 0.001$.

3. Results

3.1. Isolation of Extracellular Vesicles from NTERA2 Teratocarcinoma Cells

To investigate EV production by the human pluripotent teratocarcinoma NTERA2 cell line, we applied a differential centrifugation method to isolate two different fractions of EVs from NTERA2 conditioned culture medium, conventionally corresponding to sEVs and IEVs (Figure 1a). We analyzed by Western blot the EV preparations obtained, using antibodies to EV specific markers, both cytosolic and transmembrane, as well as the negative EV marker calnexin (Figure 1b), as recommended by MISEV 2018 [3]. Both large and small EV preparations were positive for the EV associated markers, the cytosolic heat shock protein 70 (HSP70), and the transmembrane CD63 tetraspanin, and negative for the presence of the endoplasmic reticulum-associated protein calnexin (Figure 1b).

We further analyzed NTERA2 EV preparations by scanning electron microscopy (SEM) and cryogenic transmission electron microscopy (Cryo-TEM), as reported in Figure 2. The SEM analysis highlighted the presence of particles in both IEV and sEV samples, differing in both size and abundance (Figure 2a,b,d,e). Cryo-TEM images evidenced the presence of particles delimited by a lipidic bilayer (Figure 2g–i), thereby proving that these particles were membrane-enclosed vesicles. The different Cryo-TEM images shown in the panel

confirmed the difference in size between IEVs and sEVs and showed also the heterogeneity, in terms of size and shape, inside each EV type of samples (Figure 2j–l). Interestingly, the content of IEVs was mostly opaque, suggesting the presence of electron dense material inside or on the surface of the vesicles. In particular, some IEVs also harbored inside smaller vesicles (Figure 2c).

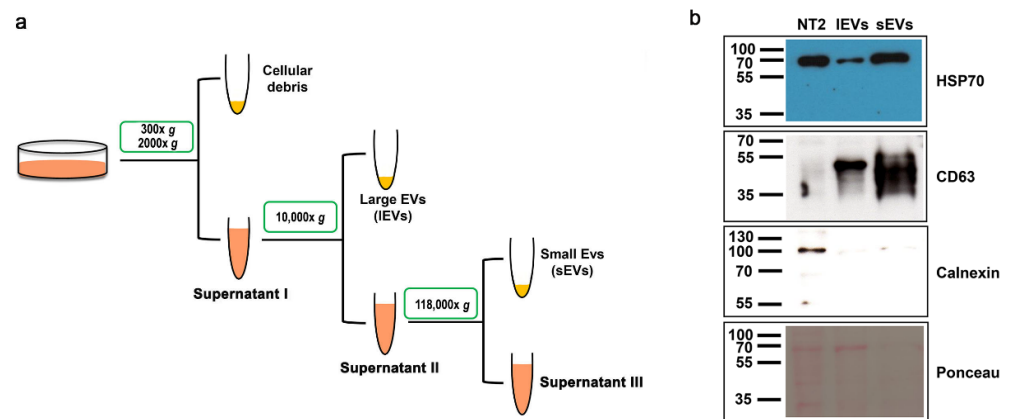


Figure 1. Isolation of extracellular vesicles from NTERA2 cells. (a) General outline of the differential centrifugation-based protocol used. (b) Protein immunoblotting with the antibody against the EV specific markers heat shock protein 70 (HSP70) and CD63, and the negative EV marker calnexin. Equal protein amounts (20 ug) of NTERA2 cell lysates (NT2), large extracellular vesicle (IEV), and small extracellular vesicle (sEV) preparations were analyzed. On the bottom: the filter after protein transfer and Red Ponceau protein revelation.

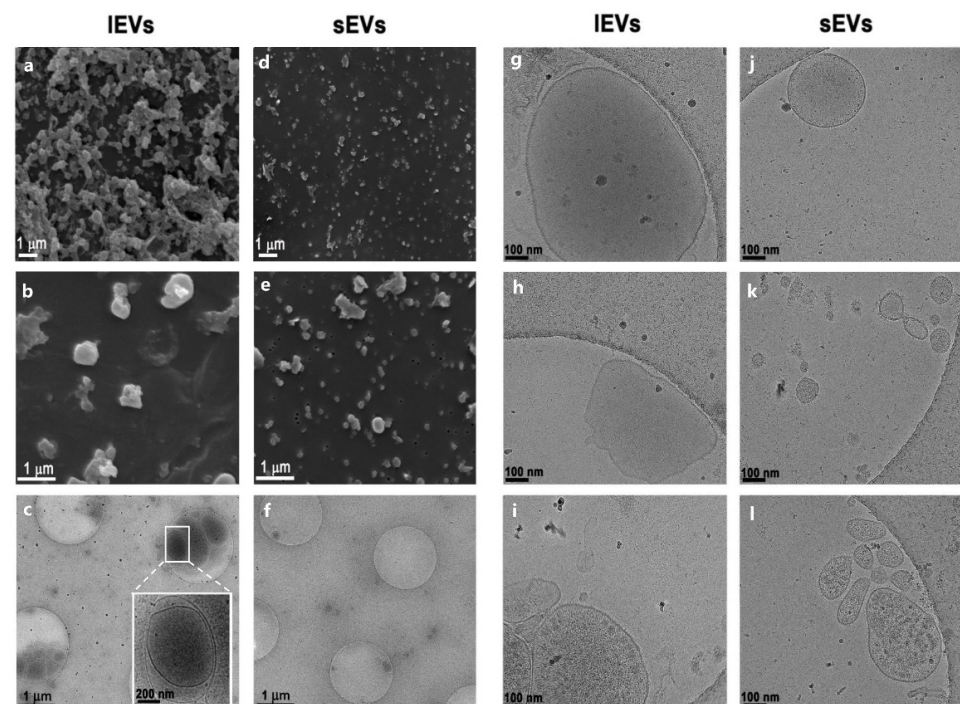


Figure 2. Analysis of NTERA2 cell-derived extracellular vesicles by electron microscopy. Scanning electron microscopy (a,b,d,e) and cryogenic transmission electron microscopy (c,f,g–l) images of large and small extracellular vesicle (IEV and sEV) preparations. Magnification bars are reported in each image.

We also characterized the NTERA2 EV preparations by NTA (Figure 3a). The NTA-profiles of the size distributions of small and large NTERA2-derived EVs indicated a

canonic distribution for the sEVs, in which the main population was about 100 nm (mean at 151 ± 3 nm), while the large EVs had a distribution in a wider size in which two other distinct populations were visible, one about 250 nm and another about 320 nm (mean at 230 ± 3 nm). From the inset histograms in Figure 3a, which show a representative result of five NTA measurements on five independent NTERA2-derived vesicle preparations, it is evident that IEVs (average concentration equal to $2.36 \times 10^{11} \pm 2.95 \times 10^{10}$ particles/mL) were 2.81 times more concentrated than the sEVs (average concentration equal to $8.42 \times 10^{10} \pm 3.01 \times 10^9$ particles/mL). All together, these data demonstrated that the preparations isolated from NTERA2 cells through the widely used differential centrifugation method truly contained vesicles. Both sEVs and IEVs were heterogeneous in size, shape, and density. Moreover, the amount of NTERA2 IEVs isolated was almost three times higher than the sEV amount.

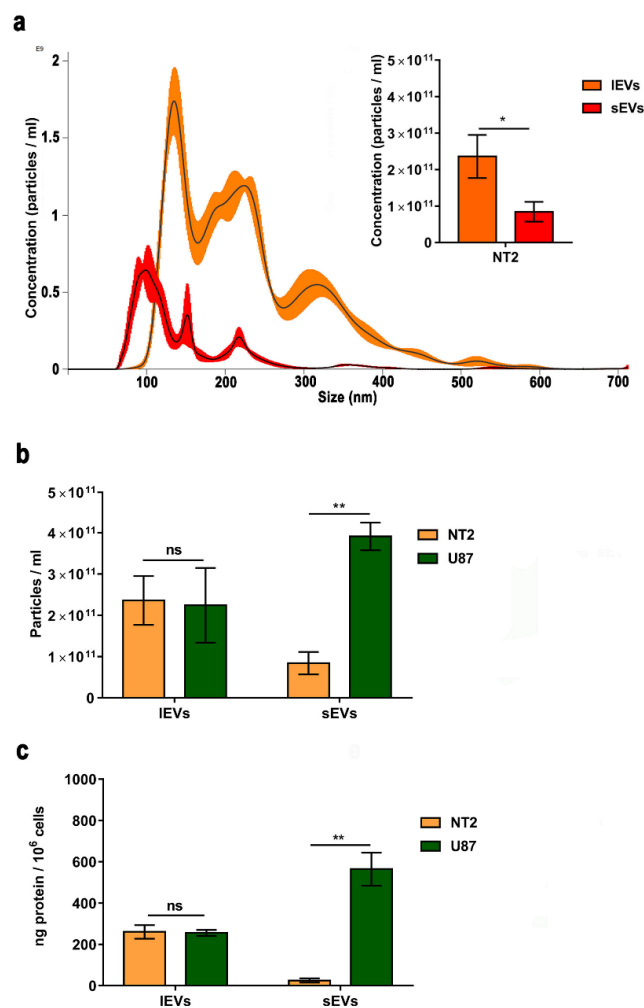


Figure 3. Extracellular vesicle quantification. (a) Nanoparticle tracking analysis (NTA) of NTERA2 extracellular vesicles. Representative image of size distribution of small extracellular vesicles or sEVs (red line) and large extracellular vesicles or IEVs (orange line). The inset histogram shows the mean \pm standard mean error of sEV and IEV concentration. (b,c) Comparison of the concentration of particles measured by NTA (b) and the protein yield (c) in sEV and IEV samples isolated from NTERA2 and U87 cancer cells. The volume of resuspension is kept constant. To determine particle concentration, five and two different samples have been analyzed for NTERA2 and U87, respectively. For each sample, five experiment videos of 60 s duration were analyzed. To determine protein yield six and three different experiments have been analyzed for NTERA2 and U87, respectively. ns not significant, * $p < 0.05$; ** $p < 0.01$.

As a comparison, we also applied the same methodology to isolate sEVs and IEVs from the U87 GBM cell line, whose EVs have been well characterized in the literature [39]. As shown in Figure 3b, the concentration of particles collected from NTERA2 and U87 cancer cell lines was very similar in the case of IEVs ($2.36 \times 10^{11} \pm 2.95 \times 10^{10}$ particles/mL and $2.24 \times 10^{11} \pm 9.06 \times 10^{10}$, respectively). Interestingly, the concentration of particles inside the NTERA2 sEV samples ($8.42 \times 10^{10} \pm 3.01 \times 10^9$ particles/mL) was significantly lower with respect to those isolated from U87 cells ($3.90 \times 10^{11} \pm 6.36 \times 10^{10}$ particles/mL). By comparing the protein yield of the EV preparations from both cancer cell cultures, we found a similar trend (Figure 3c). The protein yield of NTERA2 and U87 IEV fractions was very similar (260.4 ± 33 ng/ 10^6 cells and 255.9 ± 14.7 ng/ 10^6 cells, respectively), whereas the protein yield associated with NTERA2-derived sEVs (25.2 ± 25.3 ng/ 10^6 cells) was very much lower with respect to U87-derived sEVs (564.6 ± 79.9 ng/ 10^6 cells).

3.2. Functional Characterization of NTERA2 Large Extracellular Vesicles

Being that the IEVs isolated from NTERA2 were more abundant than the correspondent sEVs, we preferred to focus on IEV functional characterization. Therefore, we tested their effect on different tumor features, such as tumor cell migration, proliferation, and drug-sensitivity, using as a model system the well-characterized U87 human GBM cell line [40].

First, we tested the effect of IEVs on tumor cell migration, by using the wound healing assay (Figure 4a), as described in Materials and Methods. In the absence of IEVs, U87 wound closure was almost completed after 20 h. Noteworthy, the incubation of U87 GBM cells with NTERA2 IEVs affected U87 tumor cell migration. U87 cell cultures showed a delay in wound closure in the presence of IEVs, which was detectable after 6 h and even more striking after 20 h of treatment (Figure 4b). These results uncovered the ability of NTERA2 cell-derived IEVs in impairing GBM cell migration.

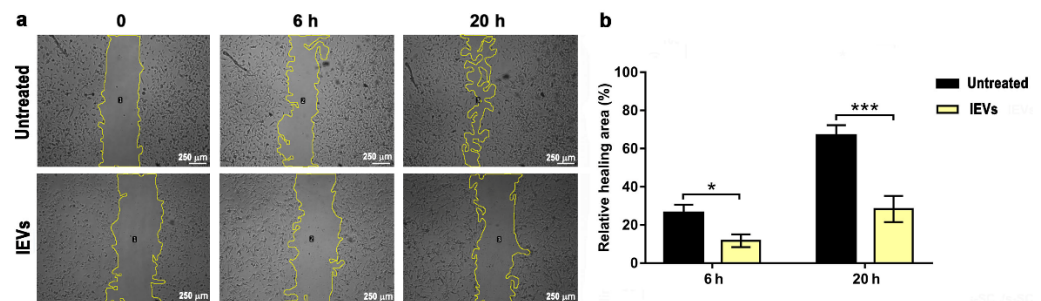


Figure 4. Wound healing assay. (a) Images of U87 cells, both untreated and treated with NTERA2 large extracellular vesicles (IEVs) were taken at 0, 6, and 20 h after wound. The open area surrounded by a yellow line is the one calculated by the ImageJ software. (b) Relative wound healing area in the different conditions. Three independent experiments were performed, each one in duplicate. Data are shown as means \pm standard error of mean. * $p < 0.05$; *** $p < 0.001$.

Then, we analyzed the effect of IEVs on GBM cell proliferation and drug sensitivity by measuring the number of viable cells in the different conditions through the CellTiter 96[®] AQueous One Solution Reagent colorimetric assay. Incubation of U87 cells with the NTERA2 IEVs for 48 and 72 h did not cause any significant variation in the absorbance measured, and then in the number of viable cells, with respect to U87 untreated cells (Figure 5a). These data indicate that IEVs did not significantly alter the U87 GBM cell proliferation rate.

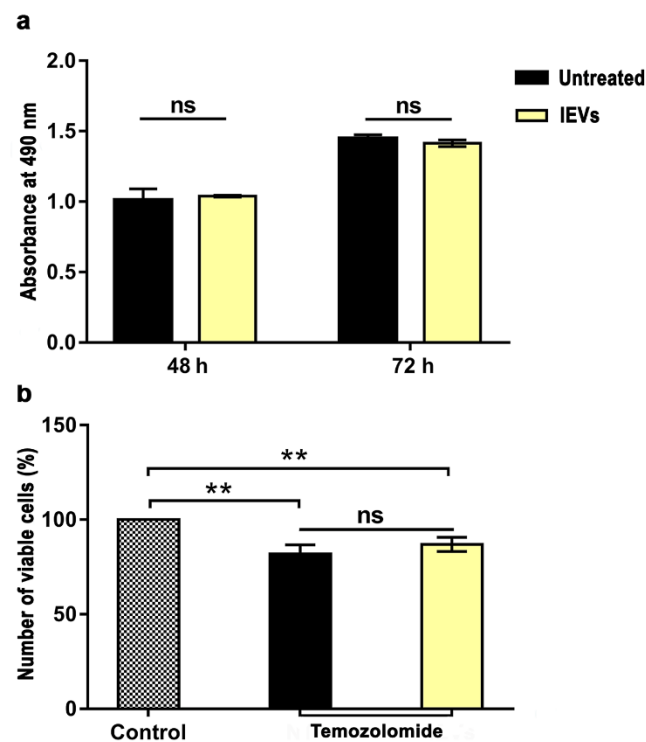


Figure 5. Cell proliferation and drug-sensitivity assay. (a) Cell proliferation assay. Absorbance of colorimetric assay of U87 cells after 48 and 72 h in absence (untreated) or presence of NTERA2 large extracellular vesicles (IEVs). No significant (ns) difference between the two samples was detected. (b) Temozolomide (TMZ) drug-sensitivity assay after 72 h of treatment, in combination or not with NTERA2 IEVs. Cell viability decreased with TMZ treatment, but no significant differences were detected between the effect caused by TMZ alone or in combination with NTERA2 IEVs. The results are shown as means \pm standard error of mean from two independent experiments, each one in duplicate. ns not significant, ** $p < 0.01$.

In the drug sensitivity assay, IEV incubation was coupled with treatment with the chemotherapeutic agent TMZ, mostly employed in GBM therapy (Figure 5b). As expected, TMZ drug treatment reduced U87 cell viability with respect to the control, but IEVs did not cause any significant change in the sensitivity of U87 GBM cells to the chemotherapeutic agent.

All together, these data point to a specific inhibitory effect of NTERA2-derived IEVs on U87 tumor cell migration, without affecting cell proliferation and sensitivity to the TMZ drug.

3.3. Association and Functional Relevance of CRIPTO in NTERA2 Extracellular Vesicles

NTERA2 cells are characterized by a strong expression of the oncofetal *CRIPTO* gene, that has been isolated precisely in these cells, and for this reason was also named *TERATOCARCINOMA DERIVED GROWTH FACTOR 1* or *TDGF1* [21,22]. First of all, we verified that in our culture conditions NTERA2 cells expressed *CRIPTO* and exposed the *CRIPTO* protein on the plasma membrane. A flow cytometry analysis (Figure 6b,c) highlighted the heterogeneity of the NTERA2 cell culture, in which it was possible to detect cells exposing on the plasma membrane different amounts of *CRIPTO* protein. By defining the gates shown in Figure 6b, it was possible to distinguish a high- and low-expressing population, corresponding approximately to the $12.55 \pm 2.35\%$ and $86.95 \pm 2.45\%$ of NTERA2 *CRIPTO* positive cells, respectively. These results might suggest a dynamic equilibrium, possibly due to modifications involving the plasma membrane, such as, for example, the known mechanism of *CRIPTO* GPI-anchor cleavage and extracellular

release or an unprecedented CRIPTO-linked mechanism of vesicle budding from the cell membrane.

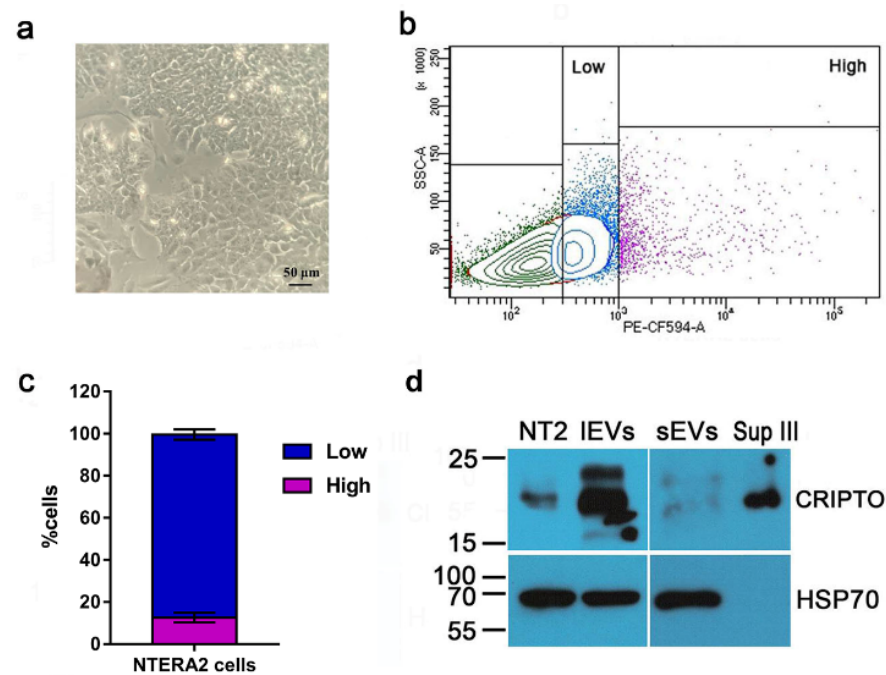


Figure 6. CRIPTO protein distribution in NTERA2 cell line. (a) Representative image of NTERA2 cell culture. (b) Flow cytometry analysis of CRIPTO protein presence on the cell membrane of NTERA2 cells. Two populations of CRIPTO positive cells (high and low), exposing different levels of the protein on the membrane, were distinguished by the respective gates. (c) Distribution of the CRIPTO high and low populations. The results are a mean of three independent experiments. (d) Equal protein amounts (20 ug) of NTERA2 cell lysates (NT2), large extracellular vesicles (IEVs), small extracellular vesicles (sEVs), and supernatant at the end of the centrifugation procedure (Sup III) were immunoblotted with an antibody against CRIPTO or against the EV marker heat shock protein 70 (HSP70).

Therefore, we analyzed by Western blot whether CRIPTO was associated to the EVs released by NTERA2 cells (Figure 6d). As expected, CRIPTO positive signals were detected in the NTERA2 cell lysate as well as in the non-particulate supernatant (Sup III) following EV separation. This finding was expected in view of the GPI-anchored nature of CRIPTO, that can be either membrane-associated or released as a soluble protein in the extracellular milieu. Noteworthy, CRIPTO was also detected in the EV preparations, both IEV and sEV, and, in particular, was strongly enriched in the IEVs (Figure 6d).

The enrichment of CRIPTO in IEVs led us to hypothesize that the CRIPTO protein might be involved in the reduction of U87 cell migration induced by NTERA2 IEVs (Figure 4). To test this hypothesis, we repeated the wound healing experiments by preincubating the IEVs with an antibody specific for CRIPTO that binds to the native CRIPTO protein. We found that preincubation with a CRIPTO antibody decreased the effect of IEVs and partially rescued cell migration (Figure 7). Preincubation with a nonspecific antibody, instead, did not cause any effect (Figure 7). We tested the effect of the preincubation of IEVs with a CRIPTO antibody also in cell proliferation and TMZ drug-sensitivity assays, and we could not find any difference with respect to pristine IEVs.

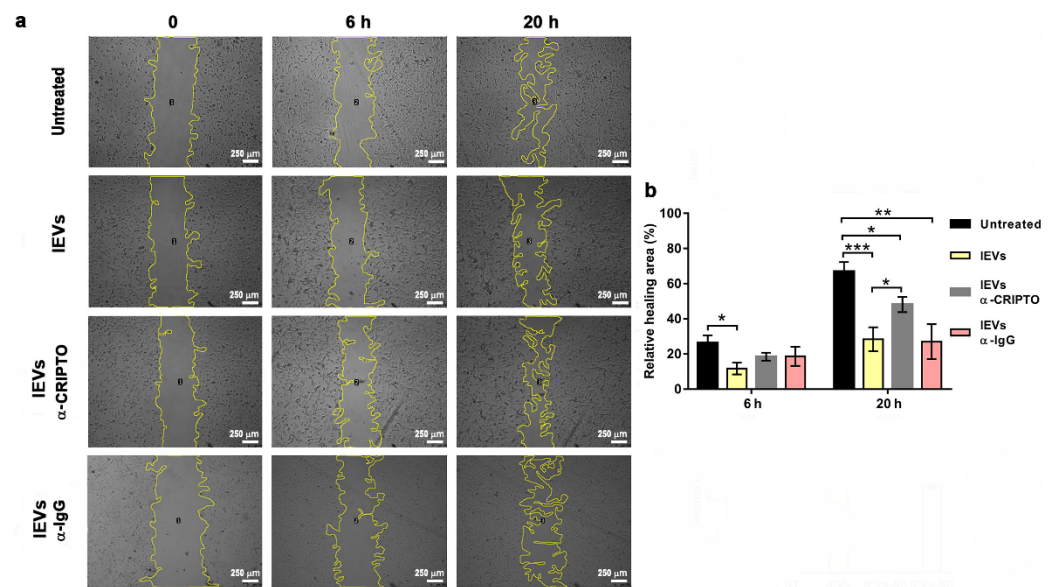


Figure 7. Rescue of U87 cell migration. (a) Cell migration at 0, 6, and 20 h of untreated U87 cells, U87 treated with NTERA2 large extracellular vesicles (IEVs) or NTERA2-IEVs previously incubated with anti-CRIPTO antibody (IEVs- α -Cripto) and a scramble antibody (IEVs- α -IgG), respectively. Open area is outlined by a yellow line and analyzed with ImageJ. (b) Relative wound healing area in the different conditions. Three independent experiments were performed, each in duplicate. Data are shown as means \pm standard error of mean. Inhibitory effect of NTERA2-IEVs was partially rescued after 20 h when vesicles were pretreated with anti-CRIPTO antibody. Rescue was not observed when anti-IgG antibody was added. * $p < 0.05$; ** $p < 0.01$; *** $p < 0.001$.

4. Discussion

Cancer cells can communicate with each other and induce phenotype changes in the recipient cells. One of the mechanisms by which they can communicate involves cancer EV release and uptake. The EV exchange between cancer cells with different phenotypic properties has been shown to transfer apoptosis resistance [41], drug resistance [42], as well as metastatic and migration properties [43]. EVs can be released by the direct outward budding and fission of the plasma membrane, and in this case are generally called microvesicles or ectosomes, or have an endocytic origin, being formed as intraluminal vesicles (ILVs) of the late endosomes or multivesicular bodies (MVBs), and then are named exosomes [2,44]. The diameter of exosomes is close to the diameter of ILVs from which they derive, therefore ranging from 30 to 100–150 nm in diameter, whereas microvesicle budding from plasmatic membrane escapes from this size restriction. Microvesicles, then, are more heterogeneous and they can be as small as exosomes or reach 1–2 μ m in diameter [2,44–46]. During interaction with target cells, components of the EV membranes can bind directly to receptors [2,47,48]. Alternatively, EV cargo is internalized into the cell through the direct fusion of the EV with the plasma membrane and the release of the EV content in the cytoplasm, or through endocytosis/phagocytosis pathways in which intact EVs fuse into the MVBs [44,49–51].

Even though NTERA2 teratocarcinoma cells have been extensively characterized, we found no study in the literature on EVs released by these cells or other teratocarcinoma cell lines. Our work isolated and characterized for the first time the EVs released by NTERA2 cells, showing a significant lower number of particles and protein yield in the sEV preparations obtained compared to the IEV ones. These data suggest that NTERA2 cells might preferentially release larger vesicles, and then led us to speculate that the preferential NTERA2 EV biogenesis mechanism might involve outer membrane budding of microvesicles, with respect to the endocytic pathway involved in generating smaller vesicles. Therefore, NTERA2 cells might be an interesting model system for the study of microvesicle biogenesis and their specific components. A cryogenic TEM revealed also the presence of

multilayered EVs which have previously been described in the literature as isolated from different sources such as blood plasma [52], semen [53], conditioned media of cultured cells [54], and also in suspensions of lipid vesicles [55]. Different mechanisms leading to the multilayered vesicles were suggested, including the nuclear or mitochondrial origin of EVs and membrane fusion or fission [53]. It should, however, be considered that multilayered EVs could be formed also due to the loss of water during sample preparation [55]. In fact, as the volume of the vesicle decreases while its surface remains constant, its relative volume decreases, and invaginations might form and develop into concentric vesicles [56].

Interestingly, our data point to a functional role of the IEVs released by NTERA2 cells on GBM development, in particular by counteracting GBM cell migration, without a notable effect on cell proliferation and chemoresistance. The effect of NTERA2 IEVs might be further investigated by using different migration assays (i.e., transwell assay) as well as in animal models to analyze their potential as migratory inhibitors of GBM cells *in vivo*.

Moreover, our findings show, for the first time, the association of the CRIPTO protein to IEVs. The ability of the antibody specific for CRIPTO to rescue the antimigratory effects induced by NTERA2 IEVs has two important implications. The first one is that CRIPTO is accessible to the antibody and then exposed on the surface of IEVs. CRIPTO is a GPI-anchored protein linked to the outer layer of the cell membrane [18,57] and localized, as with most GPI proteins, to the lipid rafts domains, characterized by a peculiar lipidic composition and involved in membrane blebbing and microvesicle release [58,59]. Therefore, the membrane GPI-anchored CRIPTO protein can be present on the surface of NTERA2 microvesicles which bud from the plasma membrane. We also found CRIPTO associated to sEV fractions, though at a lesser extent. In agreement, several studies have reported the presence of various GPI-anchored proteins also in exosomes [60]. In particular, very recently CRIPTO has been found on the surface on sEVs released by another type of cancer cell: the perihilar cholangiocarcinoma (PHCCA) cells [20]. Our analysis showing CRIPTO also in sEVs and IEVs derived from teratocarcinoma cells, coupled with the previous finding of Hu and coauthors (2021) [20], led us to hypothesize a more general mechanism that could involve many types of cancer. Noteworthy, CRIPTO might be an EV marker present on the surface of vesicles released by different types of cancer cells.

The second implication is that the IEV-associated form of CRIPTO plays a key role in the negative effect on GBM cell migration induced by NTERA2 IEVs. These findings are really intriguing, in consideration that previous studies demonstrated the ability of a functionally active recombinant soluble CRIPTO protein to stimulate the migration of different types of cells, including mammary epithelial cells and human umbilical vein endothelial cells [61–63]. The induction of CRIPTO shedding from the cell membrane by the Glycosylphosphatidylinositol-Phospholipase enzyme is also able to enhance endothelial cell migration [63]. More strikingly, most literature on CRIPTO pointed to its role as an oncofetal protein associated with increased cancer features and the worst patient prognosis [15,16,64]. However, we previously unmasked a dual role of Cripito in tumorigenesis, by showing that *Cripito* haploinsufficiency in mouse models, surprisingly, increased colon tumor formation after azoxymethane treatment [65]. These data suggested a role of Cripito in tumorigenesis that is intricately regulated and strictly dependent on the cellular context in which it acts, as well as the balance with other molecules in the same signaling pathway, such as the Glucose Regulated Protein 78 kDa (GRP78) [65].

As regards GBM, despite the first evidence of a role of CRIPTO in this type of cancer [66,67], its significance in GBM progression and pathogenesis has not been addressed so far. Recent studies focused on U87 GBM cells, in which, however, *CRIPTO* was overexpressed to study its functional effect, reporting enhanced U87 cell proliferation and migration after *CRIPTO* overexpression [68,69]. A role of CRIPTO in U87 cellular migration was also suggested by localization studies, in which, after its overexpression, the CRIPTO protein was mainly sub-localized in tunneling nanotubes, dynamic filopodia, and shed filopodia/retraction fibers [70], which are dynamic structures known to be involved in cell orientation and migration [71]. The overexpression studies definitely validated the use

of the U87 as an ideal cellular system in which to test exogenous CRIPTO activity. In our work, however, we adopted a more physiological approach based on U87 cell exposure to CRIPTO through incubation with natural EVs intrinsically strongly enriched in CRIPTO. Our findings highlight a specific role of IEV-associated CRIPTO in GBM cell migration. However, differently from previous studies, the CRIPTO-enriched IEV treatment causes a reduction in GBM cell migration. Our data add a higher grade of complexity for the fine tuning of CRIPTO localization and consequent cellular function. CRIPTO is able to interact with a plethora of molecules on the cell membrane, activating different signaling pathways and cellular responses [17,64]. The U87 cells contain most of the surface molecules to whom CRIPTO binds; in fact, they expose on the membrane the main CRIPTO interactors that are ALK4 and ALK7 receptors, being able to activate in the U87 the downstream Smad signaling pathway [72], Glypican 1 [73], as well as the Wnt co-receptors low-density lipoprotein receptor-related protein LRP5 [74], Notch1 [75], and GRP78 [76]. It would be tempting to speculate that the IEV-associated CRIPTO protein might act as a dominant negative able to bind and sequester in an inactive form the target receptor complexes on the U87 cell surface, thus altering the downstream cellular response. In a more general scenario, EV-CRIPTO might interfere with the activity of the other CRIPTO forms (the plasma membrane bound and the soluble ones), and the balance among the different CRIPTO forms might account for the resultant effect of CRIPTO as a tumor agonist or antagonist.

Interestingly, other signaling molecules that interact with CRIPTO, such as the soluble factors Transforming Growth Factor β (TGF β) or Lefty, induce a pleiotropic reaction that leads to a diverse and varied set of responses that range from cytostatic and apoptotic tumor-suppressive ones, to proliferative, invasive, angiogenic, and oncogenic ones [77–80]. The pleiotropic pathway is modulated by the cellular context and its integration with other signaling pathways [79]. In addition, TGF β itself, other ligands of the TGF β superfamily, as well as key components of the TGF β signaling machinery, including GRP78, have been found associated to EVs [81,82]. The use of alternative routes might serve the purpose of finely regulating the role of these factors in cancer development and progression. Finally, their association to EVs might also be exploited for cancer diagnostic and therapeutic purposes.

All together, our results expand the knowledge of CRIPTO localization and function, paving the way to the possible exploitation of NTERA2 CRIPTO positive EVs for GBM therapeutic approaches aimed to reduce GBM cell migration. Since migration and infiltration in healthy brain tissues constitute one of the main causes of the bad GBM prognosis, novel strategies aimed to reduce GBM cell migration might potentially have a strong impact on GBM treatment.

5. Conclusions

In this study, we isolated and characterized for the first time EVs released by the human pluripotent teratocarcinoma NTERA2 cells, uncovering the association of CRIPTO to IEVs. Furthermore, NTERA2-produced IEVs, when incubated with U87 GBM cells, are able to reduce their migration, in a CRIPTO-dependent manner, without inducing cell proliferation and chemoresistance. These results pave the way for further investigations on the development of novel therapeutic approaches to reduce GBM cell migration and enhance the effectiveness of GBM treatments, thus improving prognosis and quality of life of GBM patients.

6. Patents

Italian patent number I0197620 has been filed.

Author Contributions: Conceptualization, G.L.L.; Data curation, F.M., M.K., G.A., V.K.-I. and G.L.L.; Formal analysis, F.M. and G.A.; Funding acquisition, A.K., A.B., D.B., V.K.-I. and G.L.L.; Investigation, F.M., M.K., G.A., D.P.R., M.H. and D.B.; Methodology, F.M., M.K., M.H., D.B., A.B.Z., M.P., M.P.S. and V.K.-I.; Project administration, A.K. and G.L.L.; Resources, M.P., M.P.S., A.B., V.K.-I. and G.L.L.; Supervision, V.K.-I. and G.L.L.; Validation, F.M., D.P.R., A.K., A.B. and V.K.-I.; Visualization, F.M.,

G.A., D.P.R., V.K.-I. and G.L.L.; Writing—original draft, F.M. and G.L.L.; Writing—review and editing, F.M., G.A., A.B.Z., M.P., M.P.S., A.K., A.B., V.K.-I. and G.L.L. All authors have read and agreed to the published version of the manuscript.

Funding: This research was funded by grants from Regione Campania (PO FESR 2014–2020 SATIN) to G.L.L.; the European Union’s Horizon 2020 research and innovation programme (VES4US project, grant agreement No 801338) to A.B., A.K., V.K.I. and G.L.L.; and Slovenian Research Agency ARRS, grant numbers P3-0388, J1-9162 and J3-3066 to V.K.I., grant number P2-0132 to M.H., and grant number P1-0391 to M.P., M.K. and A.B.Z.

Data Availability Statement: Data are contained within the article. Additional data are available from the corresponding author upon reasonable request.

Acknowledgments: The authors acknowledge the fluorescence activated cell sorting (FACS) and the Integrated Microscopy facilities at IGB, and the Centre for Molecular Interactions and Structural Biology (CMISB) at the National Institute of Chemistry for the access to the cryo-TEM microscope. The authors also thank Margherita D’Angelo and Paulina Ramos for technical support, Gabriella Pocsfalvi and Marina Ciullo for precious discussions and suggestions, and Mariarosaria Aletta for bibliographic support.

Conflicts of Interest: The authors declare no conflict of interest.

References

1. Kalluri, R.; LeBleu, V.S. The Biology, Function, and Biomedical Applications of Exosomes. *Science* **2020**, *367*, eaau6977. [[CrossRef](#)] [[PubMed](#)]
2. Mantile, F.; Franco, P.; Stoppelli, M.P.; Liguori, G.L. Biological role and clinical relevance of extracellular vesicles as key mediators of cell communication in cancer. In *Biological Membrane Vesicles: Scientific, Biotechnological and Clinical Considerations. Advances in Biomembranes and Lipid Self-Assembly*; Elsevier: Amsterdam, The Netherlands, 2020; Volume 33.
3. Théry, C.; Witwer, K.W.; Aikawa, E.; Alcaraz, M.J.; Anderson, J.D.; Andriantsitohaina, R.; Antoniou, A.; Arab, T.; Archer, F.; Atkin-Smith, G.K.; et al. Minimal Information for Studies of Extracellular Vesicles 2018 (MISEV2018): A Position Statement of the International Society for Extracellular Vesicles and Update of the MISEV2014 Guidelines. *J. Extracell. Vesicles* **2018**, *7*, 1535750. [[CrossRef](#)] [[PubMed](#)]
4. Persico, M.G.; Liguori, G.L.; Parisi, S.; D’Andrea, D.; Salomon, D.S.; Minchiotti, G. Cripto in Tumors and Embryo Development. *Biochim. Biophys. Acta Rev. Cancer* **2001**, *1552*, S0304–S0419. [[CrossRef](#)]
5. Minchiotti, G.; Parisi, S.; Liguori, G.L.; D’Andrea, D.; Persico, M.G. Role of the EGF-CFC Gene Cripto in Cell Differentiation and Embryo Development. *Gene* **2002**, *287*, S0378–S1119. [[CrossRef](#)]
6. Ding, J.; Yang, L.; Yan, Y.T.; Chen, A.; Desai, N.; Wynshaw-Boris, A.; Shen, M.M. Cripto Is Required for Correct Orientation of the Anterior-Posterior Axis in the Mouse Embryo. *Nature* **1998**, *395*, 702–707. [[CrossRef](#)]
7. Xu, C.; Liguori, G.; Persico, M.G.; Adamson, E.D. Abrogation of the Cripto Gene in Mouse Leads to Failure of Postgastrulation Morphogenesis and Lack of Differentiation of Cardiomyocytes. *Development* **1999**, *126*, 483–494. [[CrossRef](#)]
8. Liguori, G.L.; Echevarría, D.; Improta, R.; Signore, M.; Adamson, E.; Martínez, S.; Persico, M.G. Anterior Neural Plate Regionalization in Cripto Null Mutant Mouse Embryos in the Absence of Node and Primitive Streak. *Dev. Biol.* **2003**, *264*, 537–549. [[CrossRef](#)]
9. Liguori, G.L.; Echevarria, D.; Bonilla, S.; D’andrea, D.; Liguoro, A.; Persico, M.G.; Martinez, S. Characterization of the functional properties of the neuroectoderm in mouse Cripto-/-embryos showing severe gastrulation defects. *Int. J. Dev. Biol.* **2004**, *53*, 549–557. [[CrossRef](#)]
10. Xu, C.; Liguori, G.; Adamson, E.D.; Persico, M.G. Specific Arrest of Cardiogenesis in Cultured Embryonic Stem Cells Lacking Cripto-1. *Dev. Biol.* **1998**, *196*, 237–247. [[CrossRef](#)]
11. Parisi, S.; D’Andrea, D.; Lago, C.T.; Adamson, E.D.; Persico, M.G.; Minchiotti, G. Nodal-Dependent Cripto Signaling Promotes Cardiomyogenesis and Redirects the Neural Fate of Embryonic Stem Cells. *J. Cell Biol.* **2003**, *163*, 303–314. [[CrossRef](#)]
12. Gershon, E.; Hadas, R.; Elbaz, M.; Booker, E.; Muchnik, M.; Kleinjan-Elazary, A.; Karasenti, S.; Genin, O.; Cinnamon, Y.; Gray, P.C. Identification of Trophoblast-Derived Cripto as an Essential Mediator of Embryo Implantation. *Endocrinology* **2018**, *159*, 1793–1807. [[CrossRef](#)]
13. Freeman, D.W.; Sousa, E.R.; Karkampouna, S.; Zoni, E.; Gray, P.C.; Salomon, D.S.; Kruithof-de Julio, M.; Spike, B.T. Whence Cripto: The Reemergence of an Oncofetal Factor in ‘Wounds’ That Fail to Heal. *Int. J. Mol. Sci.* **2021**, *22*, 10164. [[CrossRef](#)]
14. Ruggiero, D.; Nappo, S.; Nutile, T.; Sorice, R.; Talotta, F.; Giorgio, E.; Bellenguez, C.; Leutenegger, A.L.; Liguori, G.L.; Ciullo, M. Genetic Variants Modulating CRIPTO Serum Levels Identified by Genome-Wide Association Study in Cilento Isolates. *PLoS Genet.* **2015**, *11*, e1004976. [[CrossRef](#)]
15. de Castro, N.P.; Rangel, M.C.; Nagaoka, T.; Salomon, D.S.; Bianco, C. Cripto-1: An Embryonic Gene That Promoted Tumorigenesis. *Future Oncol.* **2010**, *6*, 1127–1142. [[CrossRef](#)]

16. Rodrigues Sousa, E.; Zoni, E.; Karkampouna, S.; La Manna, F.; Gray, P.C.; De Menna, M.; Kruithof-de Julio, M. A Multidisciplinary Review of the Roles of Cripto in the Scientific Literature through a Bibliometric Analysis of Its Biological Roles. *Cancers* **2020**, *12*, 1480. [[CrossRef](#)]
17. Klauzinska, M.; Castro, N.P.; Rangel, M.C.; Spike, B.T.; Gray, P.C.; Bertolette, D.; Cuttitta, F.; Salomon, D. The Multifaceted Role of the Embryonic Gene Cripto-1 in Cancer, Stem Cells and Epithelial-Mesenchymal Transition. *Semin. Cancer Biol.* **2014**, *29*, 51–58. [[CrossRef](#)]
18. Minchiotti, G.; Parisi, S.; Liguori, G.; Signore, M.; Lania, G.; Adamson, E.D.; Lago, C.T.; Persico, M.G. Membrane-Anchorage of Cripto Protein by Glycosylphosphatidylinositol and Its Distribution during Early Mouse Development. *Mech. Dev.* **2000**, *90*, S0925–S4773. [[CrossRef](#)]
19. Chu, J.; Ding, J.; Jeays-Ward, K.; Price, S.M.; Placzek, M.; Shen, M.M. Non-Cell-Autonomous Role for Cripto in Axial Midline Formation during Vertebrate Embryogenesis. *Development* **2005**, *132*, 5539–5551. [[CrossRef](#)]
20. Hu, C.; Zhang, Y.; Zhang, M.; Li, T.; Zheng, X.; Guo, Q.; Zhang, X. Exosomal Cripto-1 Serves as a Potential Biomarker for Perihilar Cholangiocarcinoma. *Front. Oncol.* **2021**, *11*, 3144. [[CrossRef](#)]
21. Ciccodicola, A.; Dono, R.; Obici, S.; Simeone, A.; Zollo, M.; Persico, M.G. Molecular Characterization of a Gene of the ‘EGF Family’ Expressed in Undifferentiated Human NTERA2 Teratocarcinoma Cells. *EMBO J.* **1989**, *8*, 1987–1991. [[CrossRef](#)]
22. Dono, R.; Montuori, N.; Rocchi, M.; De Ponti-Zilli, L.; Ciccodicola, A.; Persico, M.G. Isolation and Characterization of the CRIPTO Autosomal Gene and Its X-Linked Related Sequence. *Am. J. Hum. Genet.* **1991**, *49*, 555–565.
23. Andrews, P.W. Teratocarcinomas and Human Embryology: Pluripotent Human EC Cell Lines. Review Article. *Apmis* **1998**, *106*, 158–168. [[CrossRef](#)]
24. Furnari, F.B.; Fenton, T.; Bachoo, R.M.; Mukasa, A.; Stommel, J.M.; Stegh, A.; Hahn, W.C.; Ligon, K.L.; Louis, D.N.; Brennan, C.; et al. Malignant Astrocytic Glioma: Genetics, Biology, and Paths to Treatment. *Genes Dev.* **2007**, *21*, 2683–2710. [[CrossRef](#)]
25. Fedele, M.; Cerchia, L.; Pegoraro, S.; Sgarra, R.; Manfioletti, G. Molecular Sciences Proneural-Mesenchymal Transition: Phenotypic Plasticity to Acquire Multitherapy Resistance in Glioblastoma. *Int. J. Mol. Sci.* **2019**, *20*, 2746. [[CrossRef](#)]
26. Alcantara Llaguno, S.; Chen, J.; Kwon, C.H.; Jackson, E.L.; Li, Y.; Burns, D.K.; Alvarez-Buylla, A.; Parada, L.F. Malignant Astrocytomas Originate from Neural Stem/Progenitor Cells in a Somatic Tumor Suppressor Mouse Model. *Cancer Cell* **2009**, *15*, 45–56. [[CrossRef](#)]
27. Lee, J.H.; Lee, J.E.; Kahng, J.Y.; Kim, S.H.; Park, J.S.; Yoon, S.J.; Um, J.Y.; Kim, W.K.; Lee, J.K.; Park, J.; et al. Human Glioblastoma Arises from Subventricular Zone Cells with Low-Level Driver Mutations. *Nature* **2018**, *560*, 243–247. [[CrossRef](#)]
28. Altmann, C.; Keller, S.; Schmidt, M.H.H. The Role of SVZ Stem Cells in Glioblastoma. *Cancers* **2019**, *11*, 448. [[CrossRef](#)]
29. Almengló, C.; Caamaño, P.; Fraga, M.; Devesa, J.; Costoya, J.A.; Arce, V.M.; José Costoya, C.A. From Neural Stem Cells to Glioblastoma: A Natural History of GBM Recapitulated in Vitro. *J. Cell Physiol.* **2021**, *236*, 7390–7404. [[CrossRef](#)]
30. Tyler, M.A.; Ulasov, I.V.; Sonabend, A.M.; Nandi, S.; Han, Y.; Marler, S.; Roth, J.; Lesniak, M.S. Neural Stem Cells Target Intracranial Glioma to Deliver an Oncolytic Adenovirus in Vivo. *Gene Ther.* **2009**, *16*, 262–278. [[CrossRef](#)]
31. Li, Z.; Zhong, Q.; Liu, H.; Liu, P.; Wu, J.; Ma, D.; Chen, X.; Yang, X. Conditioned Medium from Neural Stem Cells Inhibits Glioma Cell Growth. *Cell Mol. Biol.* **2016**, *62*, 68–73. [[CrossRef](#)]
32. Attia, N.; Mashal, M.; Grijalvo, S.; Eritja, R.; Puras, G.; Pedraz, J.L. Cationic Niosome-Based HBMP7 Gene Transfection of Neuronal Precursor NT2 Cells to Reduce the Migration of Glioma Cells in Vitro. *J. Drug Deliv. Sci. Technol.* **2019**, *53*, 101219. [[CrossRef](#)]
33. Zhao, Y.; Wang, S. Human NT2 Neural Precursor-Derived Tumor-Infiltrating Cells as Delivery Vehicles for Treatment of Glioblastoma. *Hum. Gene Ther.* **2010**, *21*, 683–694. [[CrossRef](#)]
34. Romancino, D.P.; Paterniti, G.; Campos, Y.; De Luca, A.; Di Felice, V.; D’azzo, A.; Bongiovanni, A. Identification and Characterization of the Nano-Sized Vesicles Released by Muscle Cells. *FEBS Lett.* **2013**, *587*, 1379–1384. [[CrossRef](#)]
35. Lešer, V.; Drobne, D.; Pipan, Ž.; Milani, M.; Tatti, F. Comparison of Different Preparation Methods of Biological Samples for FIB Milling and SEM Investigation. *J. Microsc.* **2009**, *233*, 309–319. [[CrossRef](#)]
36. Liguori, G.L.; Kisslinger, A. Standardization and reproducibility in EV research: The support of a quality management system. In *Biological Membrane Vesicles: Scientific, Biotechnological and Clinical Considerations. Advances in Biomembranes and Lipid Self-Assembly*; Elsevier: Amsterdam, The Netherlands, 2021.
37. Bongiovanni, A.; Colotti, G.; Liguori, G.L.; Di Carlo, M.; Digilio, F.A.; Lacerra, G.; Mascia, A.; Cirafici, A.M.; Barra, A.; Lanati, A.; et al. Applying Quality and Project Management Methodologies in Biomedical Research Laboratories: A Public Research Network’s Case Study. *Accredit. Qual. Assur.* **2015**, *20*, 203–213. [[CrossRef](#)]
38. Digilio, F.A.; Lanati, A.; Bongiovanni, A.; Mascia, A.; Di Carlo, M.; Barra, A.; Cirafici, A.M.; Colotti, G.; Kisslinger, A.; Lacerra, G.; et al. Quality-Based Model for Life Sciences Research Guidelines. *Accredit. Qual. Assur.* **2016**, *21*, 221–230. [[CrossRef](#)]
39. Yekula, A.; Minciacchi, V.R.; Morello, M.; Shao, H.; Park, Y.; Zhang, X.; Muralidharan, K.; Freeman, M.R.; Weissleder, R.; Lee, H.; et al. Large and Small Extracellular Vesicles Released by Glioma Cells in Vitro and in Vivo. *J. Extracell. Vesicles* **2020**, *9*, 1689784. [[CrossRef](#)]
40. Clark, M.J.; Homer, N.; O’Connor, B.D.; Chen, Z.; Eskin, A.; Lee, H.; Merriman, B.; Nelson, S.F. U87MG Decoded: The Genomic Sequence of a Cytogenetically Aberrant Human Cancer Cell Line. *PLoS Genet.* **2010**, *6*, e1000832. [[CrossRef](#)]

41. Wojtuszkiewicz, A.; Schuurhuis, G.J.; Kessler, F.L.; Piersma, S.R.; Knol, J.C.; Pham, T.V.; Jansen, G.; Musters, R.J.P.; Van Meerlo, J.; Assaraf, Y.G.; et al. Exosomes Secreted by Apoptosis-Resistant Acute Myeloid Leukemia (AML) Blasts Harbor Regulatory Network Proteins Potentially Involved in Antagonism of Apoptosis. *Mol. Cell. Proteom.* **2016**, *15*, 1281–1298. [[CrossRef](#)]
42. Sousa, D.; Lima, R.T.; Vasconcelos, M.H. Intercellular Transfer of Cancer Drug Resistance Traits by Extracellular Vesicles. *Trends Mol. Med.* **2015**, *21*, 595–608. [[CrossRef](#)]
43. Zomer, A.; Maynard, C.; Verweij, F.J.; Kamermans, A.; Schäfer, R.; Beerling, E.; Schiffelers, R.M.; De Wit, E.; Berenguer, J.; Ellenbroek, S.I.J.; et al. In Vivo Imaging Reveals Extracellular Vesicle-Mediated Phenocopying of Metastatic Behavior. *Cell* **2015**, *161*, 1046–1057. [[CrossRef](#)]
44. Meldolesi, J. Exosomes and Ectosomes in Intercellular Communication. *Curr. Biol.* **2018**, *28*, R435–R444. [[CrossRef](#)]
45. Colombo, M.; Raposo, G.; Théry, C. Biogenesis, Secretion, and Intercellular Interactions of Exosomes and Other Extracellular Vesicles. *Annu. Rev. Cell Dev. Biol.* **2014**, *30*, 255–289. [[CrossRef](#)]
46. Minciacchi, V.R.; Freeman, M.R.; Di Vizio, D.; Sciences, B.; Angeles, L.; Diseases, U.; Children, B. The Emerging Role of Large Oncosomes. *Semin. Cell Dev. Biol.* **2016**, *40*, 41–51. [[CrossRef](#)]
47. Gabrielli, M.; Battista, N.; Riganti, L.; Prada, I.; Antonucci, F.; Cantone, L.; Matteoli, M.; Maccarrone, M.; Verderio, C. Active Endocannabinoids Are Secreted on Extracellular Membrane Vesicles. *EMBO Rep.* **2015**, *16*, 213–220. [[CrossRef](#)]
48. Denzer, K.; van Eijk, M.; Kleijmeer, M.J.; Jakobson, E.; de Groot, C.; Geuze, H.J. Follicular Dendritic Cells Carry MHC Class II-Expressing Microvesicles at Their Surface. *J. Immunol.* **2000**, *165*, 1259–1265. [[CrossRef](#)]
49. van Niel, G.; Charrin, S.; Simoes, S.; Romao, M.; Rochin, L.; Saftig, P.; Marks, M.S.; Rubinstein, E.; Raposo, G. The Tetraspanin CD63 Regulates ESCRT-Independent and -Dependent Endosomal Sorting during Melanogenesis. *Dev. Cell* **2011**, *21*, 708–721. [[CrossRef](#)]
50. Prada, I.; Amin, L.; Furlan, R.; Legname, G.; Verderio, C.; Cojoc, D. A New Approach to Follow a Single Extracellular Vesicle–Cell Interaction Using Optical Tweezers. *Biotechniques* **2016**, *60*, 35. [[CrossRef](#)]
51. Heusermann, W.; Hean, J.; Trojer, D.; Steib, E.; von Bueren, S.; Graff-Meyer, A.; Genoud, C.; Martin, K.; Pizzato, N.; Voshol, J.; et al. Exosomes Surf on Filopodia to Enter Cells at Endocytic Hot Spots, Traffic within Endosomes, and Are Targeted to the ER. *J. Cell Biol.* **2016**, *213*, 173–184. [[CrossRef](#)]
52. Arraud, N.; Linares, R.; Tan, S.; Gounou, C.; Pasquet, J.M.; Mornet, S.; Brisson, A.R. Extracellular Vesicles from Blood Plasma: Determination of Their Morphology, Size, Phenotype and Concentration. *J. Thromb. Haemost.* **2014**, *12*, 614–627. [[CrossRef](#)]
53. Höög, J.L.; Lötvall, J. Diversity of extracellular vesicles in human ejaculates revealed by cryo-electron microscopy. *J. Extracell. Vesicles* **2015**, *4*, 28680. [[CrossRef](#)]
54. Zabeo, D.; Cvjetkovic, A.; Lässer, C.; Schorb, M.; Lötvall, J.; Höög, J.L. Exosomes purified from a single cell type have diverse morphology. *J. Extracell. Vesicles* **2017**, *6*, 1329476. [[CrossRef](#)]
55. Dubochet, J.; Adrian, M.; Chang, J.-J.; Homo, J.-C.; Lepault, J.; McDowell, A.W.; Schultz, P. Cryo-electron microscopy of vitrified specimens. *Q. Rev. Biophys.* **1988**, *21*, 129–228. [[CrossRef](#)]
56. Kralj-Iglič, V.; Pocsfalvi, G.; Mesarec, L.; Šuštar, V.; Hägerstrand, H.; Iglič, A. Minimizing isotropic and deviatoric membrane energy—An unifying formation mechanism of different cellular membrane nanovesicle types. *PLoS ONE* **2020**, *15*, e0244796. [[CrossRef](#)] [[PubMed](#)]
57. Watanabe, K.; Bianco, C.; Strizzi, L.; Hamada, S.; Mancino, M.; Bailly, V.; Mo, W.; Wen, D.; Miatkowski, K.; Gonzales, M.; et al. Growth Factor Induction of Cripto-1 Shedding by Glycosylphosphatidylinositol-Phospholipase D and Enhancement of Endothelial Cell Migration. *J. Biol. Chem.* **2007**, *282*, 31643–31655. [[CrossRef](#)]
58. Hägerstrand, H.; Mrówczyńska, L.; Salzer, U.; Prohaska, R.; Michelsen, K.A.; Kralj-Iglič, V.; Iglič, A. Curvature-dependent lateral distribution of raft markers in the human erythrocyte membrane. *Mol. Membr. Biol.* **2006**, *23*, 277–288. [[CrossRef](#)] [[PubMed](#)]
59. Pollet, H.; Conrard, L.; Cloos, A.S.; Tyteca, D. Plasma membrane lipid domains as platforms for vesicle biogenesis and shedding? *Biomolecules* **2018**, *8*, 94. [[CrossRef](#)] [[PubMed](#)]
60. Vidal, M. Exosomes and GPI-Anchored Proteins: Judicious Pairs for Investigating Biomarkers from Body Fluids. *Adv. Drug Deliv. Rev.* **2020**, *161*, 110–123. [[CrossRef](#)]
61. Wechselberger, C.; Ebert, A.D.; Bianco, C.; Khan, N.I.; Sun, Y.; Wallace-Jones, B.; Montesano, R.; Salomon, D.S. Cripto-1 Enhances Migration and Branching Morphogenesis of Mouse Mammary Epithelial Cells. *Exp. Cell Res.* **2001**, *266*, 95–105. [[CrossRef](#)]
62. Bianco, C.; Adkins, H.B.; Wechselberger, C.; Seno, M.; Normanno, N.; De Luca, A.; Sun, Y.; Khan, N.; Kenney, N.; Ebert, A.; et al. Cripto-1 Activates Nodal- and ALK4-Dependent and -Independent Signaling Pathways in Mammary Epithelial Cells. *Mol. Cell Biol.* **2002**, *22*, 2586–2597. [[CrossRef](#)]
63. Watanabe, K.; Hamada, S.; Bianco, C.; Mancino, M.; Nagaoka, T.; Gonzales, M.; Bailly, V.; Strizzi, L.; Salomon, D.S. Requirement of Glycosylphosphatidylinositol Anchor of Cripto-1 for Trans Activity as a Nodal Co-Receptor. *J. Biol. Chem.* **2007**, *282*, 35772–35786. [[CrossRef](#)]
64. Bianco, C.; Rangel, M.C.; Castro, N.P.; Nagaoka, T.; Rollman, K.; Gonzales, M.; Salomon, D.S. Role of Cripto-1 in Stem Cell Maintenance and Malignant Progression. *Am. J. Pathol.* **2010**, *177*, 532–540. [[CrossRef](#)]
65. Giorgio, E.; Liguoro, A.; D’Orsi, L.; Mancinelli, S.; Barbieri, A.; Palma, G.; Arra, C.; Liguoro, G.L. Cripto haploinsufficiency affects in vivo colon tumor development. *Int. J. Oncol.* **2014**, *45*, 31–40. [[CrossRef](#)]
66. Pilgaard, L.; Mortensen, J.H.; Henriksen, M.; Olesen, P.; Sørensen, P.; Laursen, R.; Vyberg, M.; Agger, R.; Zachar, V.; Moos, T.; et al. Cripto-1 Expression in Glioblastoma Multiforme. *Brain Pathol.* **2014**, *24*, 360–370. [[CrossRef](#)]

67. Tysnes, B.B.; Sætran, H.A.; Mørk, S.J.; Margaryan, N.V.; Eide, G.E.; Petersen, K.; Strizzi, L.; Hendrix, M.J. Age-Dependent Association between Protein Expression of the Embryonic Stem Cell Marker Cripto-1 and Survival of Glioblastoma Patients. *Transl. Oncol.* **2013**, *6*, 732–741. [[CrossRef](#)]
68. Alowaidi, F.; Hashimi, S.M.; Nguyen, M.; Meshram, M.; Alqurashi, N.; Cavanagh, B.L.; Bellette, B.; Ivanovski, S.; Meedenya, A.; Wood, S.A. Investigating the Role of CRIPTO-1 (TDGF-1) in Glioblastoma Multiforme U87 Cell Line. *J. Cell. Biochem.* **2019**, *120*, 7412–7427. [[CrossRef](#)]
69. Alowaidi, F.; Hashimi, S.M.; AlQurashi, N.; Wood, S.A.; Wei, M.Q. Cripto-1 overexpression in U87 glioblastoma cells activates MAPK, focal adhesion and ErbB pathways. *Oncol. Lett.* **2019**, *18*, 3399–3406. [[CrossRef](#)]
70. Gudbergsson, J.M.; Duroux, M. Cripto-1 Localizes to Dynamic and Shed Filopodia Associated with Cellular Migration in Glioblastoma Cells. *Eur. J. Cell Biol.* **2019**, *98*, 151044. [[CrossRef](#)]
71. Kralj-Iglic, V. Stability of Membranous Nanostructures: A Possible Key Mechanism in Cancer Progression. *Int. J. Nanomed.* **2012**, *7*, 3579–3596. [[CrossRef](#)]
72. De Silva, T.; Ye, G.; Liang, Y.Y.; Fu, G.; Xu, G.; Peng, C. Nodal Promotes Glioblastoma Cell Growth. *Front. Endocrinol.* **2012**, *3*, 59. [[CrossRef](#)]
73. Su, G.; Meyer, K.; Nandini, C.D.; Qiao, D.; Salamat, S.; Friedl, A. Glypican-1 Is Frequently Overexpressed in Human Gliomas and Enhances FGF-2 Signaling in Glioma Cells. *Am. J. Pathol.* **2006**, *168*, 2014–2026. [[CrossRef](#)]
74. Bu, G.; Maksymovitch, E.A.; Geuze, H.; Schwartz, A.L. Subcellular Localization and Endocytic Function of Low Density Lipoprotein Receptor-Related Protein in Human Glioblastoma Cells. *J. Biol. Chem.* **1994**, *269*, 29874–29882. [[CrossRef](#)]
75. Kim, H.S.; Park, Y.H.; Lee, H.S.; Kwon, M.J.; Song, J.H.; Chang, I.B. Propranolol Inhibits the Proliferation of Human Glioblastoma Cell Lines through Notch1 and Hes1 Signaling System. *J. Korean Neurosurg. Soc.* **2021**, *64*, 716–725. [[CrossRef](#)]
76. Liu, K.; Tsung, K.; Attenello, F.J. Characterizing Cell Stress and GRP78 in Glioma to Enhance Tumor Treatment. *Front. Oncol.* **2020**, *10*, 608911. [[CrossRef](#)]
77. Pardali, K.; Moustakas, A. Actions of TGF- β as Tumor Suppressor and pro-Metastatic Factor in Human Cancer. *Biochim. Biophys. Acta Rev. Cancer* **2007**, *1775*, 21–62. [[CrossRef](#)]
78. Sun, G.; Shi, L.; Li, M.; Jiang, N.; Fu, L.; Guo, J. Lefty Inhibits Glioma Growth by Suppressing Nodal-Activated Smad and ERK1/2 Pathways. *J. Neurol. Sci.* **2014**, *347*, 137–142. [[CrossRef](#)]
79. Seoane, J.; Gomis, R.R. TGF- β family signaling in tumor suppression and cancer progression. *Cold Spring Harb. Perspect. Biol.* **2017**, *9*, a022277. [[CrossRef](#)]
80. Matsumoto, T.; Chino, H.; Akiya, M.; Hashimura, M.; Yokoi, A.; Tochimoto, M.; Nakagawa, M.; Jiang, Z.; Saegusa, M. Requirements of LEFTY and Nodal Overexpression for Tumor Cell Survival under Hypoxia in Glioblastoma. *Mol. Carcinog.* **2020**, *59*, 1409–1419. [[CrossRef](#)]
81. Rodrigues-Junior, D.M.; Tsigoti, C.; Lim, S.K.; Heldin, C.-H.; Moustakas, A. Extracellular Vesicles and Transforming Growth Factor β Signaling in Cancer. *Front. Cell Dev. Biol.* **2022**, *10*, 761. [[CrossRef](#)]
82. Schneider, M.; Winkler, K.; Kell, R.; Pfaffl, M.W.; Atkinson, M.J.; Moertl, S. The Chaperone Protein GRP78 Promotes Survival and Migration of Head and Neck Cancer After Direct Radiation Exposure and Extracellular Vesicle-Transfer. *Front. Oncol.* **2022**, *12*, 842418. [[CrossRef](#)]